Inverse estimation of the permeability of porous materials using experimental data via reflected waves at low frequencies

A Berbiche, Mustapha Sadouki, Z.E.A Fellah, Erick Ogam, Mohamed Fellah, Farid G. Mitri, Claude Depollier

Inverse estimation of the permeability of porous materials using experimental data via reflected waves at low frequencies.

A. Berbiche

Laboratoire de Physique Théorique, Faculté de Physique, USTHB, BP 32 El Alia, Bab Ezzouar 16111, Algérie.

Laboratoire de Physique Théorique, Faculté de Physique, USTHB, BP 32 El Alia, Bab Ezzouar 16111, Algérie.

M. Sadouki

Faculté des Sciences et Technique, Université de Khemis Miliana BP 44225 Ain Defla, Algérie.

Z.E.A. Fellah and E. Ogam

LMA, CNRS, UPR 7051, Aix-Marseille Univ, Centrale Marseille, F-13402 Marseille Cedex 20, France

M. Fellah

Laboratoire de Physique Théorique, Faculté de Physique, USTHB, BP 32 El Alia, Bab Ezzouar 16111, Algérie.

F.G. Mitri

Chevron, Area 52 - ETC, 5 Bisbee Ct., Santa Fe, New Mexico 87508, United States.

C. Depollier

LUNAM Universite du Maine. UMR CNRS 6613 Laboratoire d'Acoustique de l'Universite du Maine UFR STS Avenue O. Messiaen 72085 Le Mans CEDEX 09 France. [1]

1. Present : MPEI, Krasnokazarmennaya 14 Moscow 111250 Russia.

An acoustic reflectivity method is proposed for measuring the permeability or flow resistivity of air-saturated porous materials. In this method, a simplified expression of the reflection coefficient is derived in the Darcy's regime (low frequency range), which does not depend on frequency and porosity. Numerical simulations show that the reflection coefficient of a porous material can be approximated by its simplified expression obtained from its Taylor development to the first order. This approximation is good especially for resistive materials (of low permeability) and for the lower frequencies. The permeability is reconstructed by solving the inverse problem using waves reflected by plastic foam samples, at different frequency bandwidths in the Darcy regime. The proposed method has the advantage of being simple compared to the conventional methods that use experimental reflected data, and is complementary to the transmissivity method which is more adapted to low resistive materials (high permeability).

I. INTRODUCTION

The acoustic characterization of air saturated porous media[1–5] is very important for the prediction of sound propagation in such media. Indeed, these materials are widely used to reduce noise in buildings, vehicles and aircraft.

Several non-acoustic parameters[1,2,6] describe sound propagation in air-saturated porous materials. The physics of acoustic wave propagation in porous materials is different depending on the frequency domain. The high and low frequency ranges[1,2,6] are defined by comparing the viscous and thermal skin thicknesses $\delta = (2\eta/\omega\rho)^{1/2}$ and $\delta' = (2\eta/\omega\rho P_r)^{1/2}$ with the effective radius of the pores r (ρ is the density of the saturating fluid ; ω the pulsation frequency ; P_r the Prandtl number and η is the fluid viscosity). The high frequency domain is defined when the viscous[6] and thermal[1] skin thicknesses are small compared to the pore radius. Otherwise, it is the low frequency domain. In the Darcy's regime (flow without inertial effect) corresponding to low frequencies[7], the viscous static permeability k_0 is the most important parameter describing the viscous losses caused by the fluid/structure exchanges. This parameter is related to the specific flow resistivity[3,5] σ by the relation : $k_0 = \eta/\sigma$. In the high frequency range, the main parameters in this domain are the tortuosity[1], viscous[6] and thermal characteristic lengths[1,3].

Among the methods[3–5,7–24] developed to measure the permeability or the flow resistivity, we distinguish between the so-called direct methods[5,8–12] which do not use sound waves, and the indirect methods[13–24] that use sound waves transmitted or reflected by the porous material. The practical implementation of the direct methods could be both complex and expensive. In this paper we propose to measure the viscous permeability (and resistivity) by developing a simple method using experimental data of transient waves reflected from samples of air saturated porous materials in a tube. The advantage of this method is the use of a simplified expression of the reflection coefficient which does not depend on the frequency or the porosity of the material. Let us recall that the classical methods[19] using the reflected waves requires the prior

knowledge of the porosity of the material, using an expression of the reflection coefficient which depends on the frequency and porosity. We show in this study that the proposed method is especially well adapted for resistive porous materials at low frequencies. In this approach, a tube is used for the acoustic propagation of transient waves. A single microphone[7,19–21] is used for the measurement of experimental signals, therefore, no calibration is required. Other techniques use an impedance tube, in which standing waves are generated, and where two[13–17] or three[18] microphones are used for experimental measurements. In this case, a calibration of the microphones is necessary for a good quality of the results. This acoustic reflectivity method is an alternative to the transmissivity method developed recently[7], which is adapted to porous materials of low resistivity (high permeability).

II. EQUIVALENT FLUID MODEL

The most general and complete theory for the description of acoustic propagation in porous media is the Biot's[25] theory. This model treats both individual and coupled behavior of the frame and pore fluid. Energy loss is considered to be caused by the viscosity of the pore fluid as it moves relative to the frame. The theory predicts two compressional waves : a fast wave, where the fluid and solid move in phase, and a slow wave where fluid and solid move out of phase. Generally, when the sound wave propagates through a porous material saturated with air, the structure remains stationary and non-deformable with respect to the acoustic excitation[1,2]. The vibrations of the solid frame can often be neglected in the absence of direct contact with the sound source, so that the waves can be considered to propagate only in fluid. This case is described by the equivalent-fluid model[1,2,6,7], which is a particular case of the Biot model, in which fluid-structure interactions are taken into account in two frequency response factors : the dynamic tortuosity of the medium $\alpha(\omega)$ given by Johnson *et al*[6], and the dynamic compressibility of the air in the porous material $\beta(\omega)$ given by Allard *et al*[1]. In the frequency domain, these factors multiply the

density of the fluid as well as its compressibility and represent the deviation from the behavior of the fluid in free space as the frequency increases. Specifically, in the low frequency domain, the viscous effects are important in all the pore volume, and the compression dilatation cycle in the porous material is slow enough to favor the thermal interactions between fluid and structure[2]. At the same time the temperature of the frame is practically unchanged by the passage of the sound wave because of the high value of its specific heat : the frame acts as a thermostat[2]. In addition, the thermal conductivity of the solid is high, and the excess heat is immediately evacuated by the solid, which therefore remains at the same temperature during the compression dilatation cycle[1,2]. In the Darcy's regime[7,26,27] (very low-frequency approximation), the expressions of the response factors $\alpha(\omega)$ and $\beta(\omega)$ when $\omega \to 0$ are given by the relations[26] :

$$\alpha(\omega) = -\frac{\eta\phi}{\rho k_0 j\omega}, \qquad \beta(\omega) = \gamma. \tag{1}$$

where k_0 is the static permeability, ϕ the porosity and γ the adiabatic constant.

Consider a homogeneous porous material that occupies the region $0 \leq x \leq L$. A sound pulse impinges normally on the medium. It generates an acoustic pressure field p and an acoustic velocity field v within the material. These acoustic fields satisfy the following equivalent-fluid macroscopic equations (along the $x-$axis)[1] :

$$\rho\alpha(\omega)j\omega v = \frac{\partial p}{\partial x}, \qquad \frac{\beta(\omega)}{K_a} j\omega p = \frac{\partial v}{\partial x}, \tag{2}$$

where, $j^2 = -1$, ρ is the saturating fluid density and K_a is the compressibility modulus of the fluid.

The incident $p^i(t)$ and reflected $p^r(t)$ fields are related in the time domain by the reflection scattering operator[19,20] R :

$$p^r(x,t) = \int_0^t R(\tau) p^i\left(t - \tau + \frac{x}{c_0}\right) d\tau. \tag{3}$$

The temporal operator kernel R is calculated by taking the inverse Fourier transform of the

reflection coefficient of a slab of porous material given by (Appendix. A) :

$$\tilde{R}(\omega) = \frac{\left(1 - Y^2(\omega)\right) \sinh\left(j\kappa(\omega)L\right)}{2Y(\omega)\cosh\left(j\kappa(\omega)L\right) + \left(1 + Y^2(\omega)\right)\sinh\left(j\kappa(\omega)L\right)}, \tag{4}$$

where :

$$Y(\omega) = \phi\sqrt{\frac{\beta(\omega)}{\alpha(\omega)}}, \qquad \text{and} \qquad \kappa(\omega) = \omega\sqrt{\frac{\rho\alpha(\omega)\beta(\omega)}{K_a}}.$$

Using the expressions (1) of the dynamic tortuosity and compressibility, we obtain the following expression for the reflection coefficient :

$$\tilde{R}(\omega) = \frac{\left(1 - C_1^2\omega\right) \sinh\left(LC_2\sqrt{j\omega}\right)}{2C_1\sqrt{j\omega}\cosh\left(LC_2\sqrt{j\omega}\right) + \left(1 + C_1^2 j\omega\right)\sinh\left(LC_2\sqrt{j\omega}\right)}, \tag{5}$$

where

$$C_1 = \sqrt{\frac{\gamma\rho k_0\phi}{\eta}}, \qquad C_2 = \sqrt{\frac{\gamma\eta\phi}{K_a k_0}} \tag{6}$$

By doing the Taylor series expansion of the reflection coefficient (Appendix. B), when the frequency tends to zero ($\omega \to 0$), we obtain :

$$\tilde{R}(\omega) = \left(\frac{1}{1 + \frac{2C_1}{LC_2}}\right)\left[1 - j\frac{\omega}{\omega_c} + ...\right], \tag{7}$$

where :

$$\omega_c = \frac{3\left(1 + \frac{2C_1}{LC_2}\right)}{2LC_1C_2\left(1 + \frac{3C_1}{LC_2} + 3\frac{C_1^2}{L^2C_2^2}\right)}. \tag{8}$$

As a first approximation, at very low frequencies, the reflection coefficient (7) is given by the first term :

$$\tilde{R} = \frac{1}{1 + \frac{2C_1}{LC_2}} = \frac{1}{1 + \frac{2k_0}{L\eta}\sqrt{\rho K_a}} \tag{9}$$

This simplified expression of the reflection coefficient is independent of the frequency and porosity of the material, and depends only on its static permeability.

Figure 1 shows the variation of the modulus of the reflection coefficient (Eq. 5) with the porosity,

for different frequencies. In this figure, a comparison is given between the two expressions of the reflection coefficients given by Eq.(9) and Eq.(5), respectively. It can be seen that for the low frequencies, the two reflection coefficients coincide.

The modulus of the reflection coefficient (7) is given by

$$\mid \tilde{R}(\omega) \mid = \left(\frac{1}{1 + \frac{2C_1}{LC_2}} \right) \sqrt{\left(1 + \left(\frac{\omega}{\omega_c} \right)^2 \right)} \tag{10}$$

Let us study the values of ω/ω_c and $\mid \tilde{R}(\omega) \mid$ for various values of frequency and of flow resistivity. For the approximation (9) of the reflection coefficient to be valid, it is necessary that ω/ω_c be very small compared to 1. Table I shows values of ω/ω_c and $\mid \tilde{R}(\omega) \mid$ for various values of frequency and flow resistivity for a porous medium of thickness $L = 5$cm and porosity $\phi = 0.9$. It can be seen that for the same value of the flow resistivity, the values of $\mid \tilde{R}(\omega) \mid$ are almost constant and those of ω/ω_c are small compared to 1, especially for low frequencies and high resistivities.

Note that the "smallness" condition obtained when $\omega/\omega_c \ll 1$ is different from the one used in the relations (1) of the dynamic tortuosity and compressibility. According to what is postulated in Ref. 27 and later mathematically justified in Ref. 28, the dynamic tortuosity $\alpha(\omega)$ can have pole-expansion with one of the poles very close to 0. This distance is the 'smallness' implied by Eq. (1).

In the time domain, the expression of the reflection operator defined by Eq. (3) is given by :

$$R(t) = \left(\frac{1}{1 + \frac{2k_0}{L\eta}\sqrt{\rho K_a}} \right) \delta(t), \tag{11}$$

where $\delta(t)$ is the Dirac function.

In the next paragraph, we compare the expression (5) of the reflection coefficient, with its simplified expression (9), using numerical simulations of signals (Eq. 3) reflected by a slab of air-saturated porous material.

III. NUMERICAL SIMULATION

Consider two samples F1 and F2 of air-saturated plastic foam, having the same thickness and porosity, respectively ; $L = 5$ cm, and $\phi = 0.9$. The permeability of these two samples takes two different values. F1 is less resistive (more permeable) than F2. The international system of units for permeability is m^2. A practical unit for permeability is the Darcy (D), (1 Darcy $=0.97 \times 10^{-12} m^2$). The permeability value of F1 is : $k_0 = 6185.6D$; (flow resistivity : $\sigma = 3000$ N m^{-4}s), and of F2 ; $k_0 = 61.86D$ (flow resistivity : $\sigma = 3.10^5$ N m^{-4}s) . In this paragraph, a comparison between simulated reflected signals computed with different expressions of the reflection coefficients (Eqs. 5 and 9) is given for the samples F1 and F2. We show under which conditions we can use the simplified expression of the reflection coefficient (Eq. 9), instead of using the more general expression (frequency dependent, Eq. 5). Fig. 1 shows a comparison between two simulated reflected signals computed with different expressions of the reflection coefficients for sample F1. The frequency bandwidth of the incident signal used for this first numerical simulation is (300-600)Hz. The first signal (solid line) corresponds to the simulated reflected signal using expression (5) of the reflection coefficient, and the second one (dashed line) using the relation (9). We note that for this frequency range (300-600)Hz, the reflected waves predicted by the two terms of the reflection coefficient are significantly different. An important shift is observed between the two signals ; 40% for the amplitude, and 0.6% for the phase. By making the same comparison with sample F2, which is less permeable than F1, the results given in figure 2 show a slight difference between the two simulated signals (shift of 10% for the amplitude, and of 0.05% for phase). We can conclude that the approximation (9) of the reflection coefficient is much more accurate when the porous medium is less permeable (more resistive).

Another test is performed by taking an incident signal with lower frequencies (40-70)Hz. The reflected signals calculated from equations (5) and (9), are compared in figures 3 and 4, for samples F1 and F2, respectively, in the frequency domain (40-70)Hz. These comparisons

show a very good agreement, since it is practically impossible to distinguish between the two curves corresponding to F1 and F2. Indeed, the simplified expression of the reflection coefficient given by equation (9) is developed in very low frequencies. This study showed that the simplified expression (9) gives the same results as expression (5) for the lower frequencies, especially for the less permeable (more resistive) materials. It would be more advantageous to use the simplified expression (Eq. 9) of the reflection coefficient, since it does not depend on the frequency or porosity, and is simpler.

IV. INVERSION OF EXPERIMENTAL REFLECTED DATA

The study presented in the previous section shows that the reflection coefficient at low frequency range can be simplified to an expression which is independent of frequency and porosity. This approximation of the reflection coefficient is even more valuable when the porous medium is resistive, i.e., with low permeability. Therefore, the simplified expression of the reflection coefficient depends only on the permeability of the material. In this part of this work, we show how to characterize a porous material saturated with air in the low frequency regime, by solving the inverse problem using experimental data of reflected waves. The simplified expression of the reflection coefficient will be used to obtain the permeability of the porous medium.

The basic inverse problem associated with a slab of porous material may be stated as follows : from the measurement of the signals reflected outside the slab, the objective is to characterize the medium. Our aim is to determine the static viscous permeability k_0 of the material by solving the inverse problem for waves reflected by the slab of porous material. The inverse problem is to find the permeability of the material which minimizes the function

$$U(k_0) = \int_0^t \left(p^r(x,t) - p^r_{exp}(x,t)\right)^2, \tag{12}$$

where $p^r(x,t)$ is the reflected wave predicted by Eq. 3 and $p^r_{exp}(x,t)$ is the experimentally determined reflected signal. The analytical method of solving the inverse problem using the

conventional least-square method is tedious. A numerical solution of the least-square method can be found which minimizes

$$U(k_0) = \sum_{i=1}^{i=N} (p^r(x,t_i) - p^r_{exp}(x,t_i))^2, \tag{13}$$

wherein $p^r(x,t_i)_{i=1,2,...N}$ is the discrete set of values of the simulated reflected signal and $p^r_{exp}(x,t_i)_{i=1,2,...N}$ is the discrete set of values of the experimental reflected signal.

The experimental setup[19] is shown in Fig. 5. The tube length is adaptable to avoid reflection, and to permit the propagation of transient signals, according to the desired frequency range. For measurements in the frequency range (20-100)Hz, a length of 50m is sufficient but it is useful to use an anechoic device placed at the end of the pipe. It is not important to keep the pipe straight ; it can be rolled in order to save space without perturbations on experimental signals. The tube diameter is 5 cm (the cut-off of the tube $f_c \sim$ 4kHz). A sound source Driver unit "Brand" constituted by loudspeaker Realistic 40-9000 is used. Tone-bursts are provided by Standard Research Systems Model DS345-30MHz synthesized function generator. The signals are amplified and filtered using model SR 650-Dual channel filter, Standford Research Systems. The signals (incident and reflected) are measured using the same microphone (Bruel & Kjaer, 4190). The incident signal is measured by putting a total reflector[19] in the same position as the porous sample.

The inverse problem is solved for four cylindrical samples of plastic foam M1, M2, M3 and M4 (M1-M4) of a diameter of 5 cm. Their porosities and thicknesses are given in Table II. The permeability values obtained by classical methods[5,10,7,19,20] are marked by $*$ in Tables III, IV, V and VI. The permeability is inverted using experimental signals reflected by the porous material samples (M1-M4). The variations in the cost function present one clear minimum corresponding to the solution of the inverse problem. Figs 6-9 show the variation of the cost function U when varying the permeability in different frequency bandwidths, for the samples (M1-M4). The results of the inverse problem are summarized in Tables III, IV, V and VI, in which inverted values of

permeability are given for different frequency bandwidths (not marked values). A comparisons between inverted permeability values obtained using the simplified expression (Eq. 9) of the reflection coefficient and its general expression (Eq.4) are given in Tables III, IV, V and VI. The average values of these inverted data are marked by $\sharp$ in Tables III-VI, for each porous sample. From these tables, it can be seen that the inverted values of permeability obtained using the simplified expression of the reflection coefficient (Eq. 9) are close to those obtained using its general expression (Eq.4). In addition, the averaged values of the optimized permeabilities (k_0) are also close to those obtained using classical methods (marked by $*$).

We noticed that the experimental data for the lower frequencies contain much more noise relative to other measures. This is why we decided to expand the measures on small frequency bands (40-120)Hz, where the approximation of the reflection coefficient is still valid. These small frequency bands have been used in the inversion process to trace different minimization curves, in the aim to obtain an good average value for the inverted permeability. The much higher frequencies for which the approximation of the coefficient reflection is not valid were not taken into account in the inversion.

The standard deviations of the experimental inverted values of the permeability are evaluated in Table VII for samples M1-M4. From this table, we can see that sample M3 has the smallest standard deviation compared to the other samples. Indeed, sample M3 has the lowest permeability value, and is therefore the most resistive material. We also see from Table VII that as long as the samples are resistive (with low permeability), the standard deviation is low. This experimental study shows that the inversion on the experimental data is particularly good and accurate as the medium is more resistive, and thus less permeable. This result confirms the validity of the theory of the reflection coefficient that we developed in the previous paragraph.

A comparison between an experimental reflected signal and simulated reflected signal is given in Figs. 10 (a-d) for the optimized values of the inverted permeabilities of the porous samples (M1-M4), respectively. The frequency bandwidth of the incident signals is (40-60)Hz. It can be

seen that the agreement between experiment and theory is good for all the samples, especially for the most resistive materials (M1) and (M3). This comparison has also been carried out in other frequency bandwidth for higher frequencies(90-120) Hz, in Figs. 11 (a-d), for samples (M1-M4), respectively. In this case, the agreement between experiment and theory for the M2 and M4 foams (less resistive and therefore more permeable) is not as good as it is with samples M1 and M3. This comparison of experimental and theoretical data of the reflected waveform shows that the inversion results are best suited for the most resistive materials and at low frequencies, which are the necessary conditions for applying the proposed method.

This method is complementary to the one using transmitted waves[7]. Its advantage is that it is well suited to porous resistive materials (low permeability), while the transmission method[7] is better for low resistive materials (high permeability). Moreover, in this approach, the knowledge of the porosity of the material is not necessary as is the case of classical methods[19] using the reflected waves.

V. CONCLUSION

In this paper, an experimental determination of the viscous permeability is given by solving the inverse problem using experimental reflected signals. The model is based on a simplified expression of the reflection coefficient obtained by Taylor expansion when the frequency tends to zero. The simplified expression of the reflection coefficient is independent of frequency and porosity, thus making the inversion process straightforward. Four plastic foam samples having different values of permeability are tested using this proposed method. The results are satisfactory especially for resistive porous materials and for the lower frequencies, which are the necessary conditions for using this model. This method opens new perspectives for the acoustic characterization of resistive porous materials which are generally difficult to characterize using transmitted waves[7]. The transmission method is more adapted for less resistive porous materials.

This study shows that the reflected waves are a good tool for the acoustic characterization of resistive porous materials in the low frequency range (Darcy's regime).

AKNOWLEDGEMENT

The authors acknowledge constructive comments from anonymous reviewers.

C. Depollier is supported by the Russian Science Foundation under grant 14-49-00079.

APPENDIX A :REFLECTION AND TRANSMISSION COEFFICIENTS

The expression of a pressure wave incident plane, with unit amplitude, at normal incidence is given by :

$$p^i(x,t) = e^{-j(\kappa x - \omega t)}, \qquad \text{where} \qquad \kappa = \frac{\omega}{c_0} = \omega\sqrt{\frac{\rho}{K_a}},$$

κ is the wave number of the free fluid. In the medium (I) ($x < 0$), the movement results from the superposition of incident and reflected waves (Fig. 12) :

$$p_1(x,t) = e^{-j(\kappa x - \kappa t)} + Re^{-j(-\kappa x - \omega t)}, \tag{14}$$

where R is the reflection coefficient. According to Eq. 2, the expression of the velocity field in the medium (I) wrote :

$$v_1(x,t) = \frac{1}{Z_f}\left(e^{-j(\kappa x - \omega t)} - R(\omega)e^{-j(-\kappa x - \omega t)}\right), \qquad \text{where} \qquad Z_f = \sqrt{\rho K_a}. \tag{15}$$

In the medium (II) corresponding to the porous material, the expressions of the pressure and velocity fields are :

$$p_2(x,t) = A(\omega)e^{-j(\kappa(\omega)x - \omega t)} + B(\omega)e^{-j(-\kappa(\omega)x - \omega t)}, \tag{16}$$

$$v_2(x,t) = \frac{1}{Z(\omega)}\left(A(\omega)e^{-j(\kappa(\omega)x - \omega t)} - B(\omega)e^{-j(-\kappa(\omega)x - \omega t)}\right) \tag{17}$$

In these expressions $A(\omega)$ and $B(\omega)$ are function of pulsation for determining, $Z(\omega)$ and $\kappa(\omega)$ are the characteristic impedance and the wave number, respectively, of the acoustic wave in the porous medium. These are two complex quantities :

$$\kappa(\omega) = \omega\sqrt{\frac{\rho\alpha(\omega)\beta(\omega)}{K_a}}, \qquad Z(\omega) = \sqrt{\frac{\rho K_a \alpha(\omega)}{\beta(\omega)}}$$

Finally, in the medium (III), the expressions of the pressure and velocity fields of the wave transmitted through the porous material are :

$$p_3(x,t) = \tilde{T}(\omega)e^{-j(\kappa(x-L) - \omega t)}, \tag{18}$$

$$v_3(x,t) = \frac{1}{Z_f}\tilde{T}(\omega)e^{-j(\kappa(x-L) - \omega t)}, \tag{19}$$

where $\tilde{T}(\omega)$ is the transmission coefficient. To determine the coefficients of reflection and transmission, the continuity conditions are written to the interfaces $x = 0$ and $x = L$ of the porous medium :

$$p_1(0^-) = p_2(0^+), \quad p_2(L^-) = p_3(L^+), \quad v_1(0^-) = \phi v_2(0^+), \quad \phi v_2(L^-) = v_3(L^+). \tag{20}$$

Using expressions (20) and relations (14-19), we obtain the following relations between $A(\omega)$, $B(\omega)$, $R(\omega)$ and $T(\omega)$:

$$1 + R(\omega) = A(\omega) + B(\omega), \quad \tilde{T} = A(\omega)e^{-j\kappa(\omega)L} + B(\omega)e^{j\kappa(\omega)L},$$
$$1 - R(\omega) = \phi\frac{Z_f}{Z(\omega)}\left(A(\omega) - B(\omega)\right), \quad \tilde{T}(\omega) = \phi\frac{Z_f}{Z(\omega)}\left(A(\omega)e^{-j\kappa(\omega)L} - B(\omega)e^{j\kappa(\omega)L}\right).$$

The solution of this system of equations gives the expressions of the reflection and transmission coefficients :

$$R(\omega) = \frac{\left(1 - Y^2(\omega)\right)}{\left(1 + Y^2(\omega)\right) + 2Y(\omega)\coth\left(j\kappa(\omega)L\right)}$$
$$\tilde{T}(\omega) = \frac{2Y(\omega)}{2Y(\omega)\cosh\left(j\kappa(\omega)L\right) + \left(1 + Y^2(\omega)\right)\sinh\left(j\kappa(\omega)L\right)},$$

where :

$$Y(\omega) = \phi\sqrt{\frac{\beta(\omega)}{\alpha(\omega)}}.$$

APPENDIX B : TAYLOR EXPANSION OF THE REFLECTION COEFFICIENT

The reflection coefficient $\tilde{R}(\omega)$ is given by (5) :

$$\begin{aligned}\tilde{R}(\omega) &= \frac{\left(1-C_1^2 j\omega\right)\sinh\left(LC_2\sqrt{j\omega}\right)}{2C_1\sqrt{j\omega}\cosh\left(LC_2\sqrt{j\omega}\right)+\left(1+C_1^2 j\omega\right)\sinh\left(LC_2\sqrt{j\omega}\right)},\\ &= \left(\frac{1-C_1^2 j\omega}{1+C_1^2 j\omega}\right)\left[\frac{1}{1+\frac{2C_1\sqrt{j\omega}}{\left(1+C_1^2 j\omega\right)}\coth(LC_2\sqrt{j\omega})},\right]\end{aligned}$$

where $C_1$and C_2 are given by Eq. 6.

The Taylor series expansion in the vicinity of zero of $\left(\frac{1-C_1^2 j\omega}{1+C_1^2 j\omega}\right)$, $\frac{2C_1\sqrt{j\omega}}{\left(1+C_1^2 j\omega\right)}$ and $\coth(LC_2\sqrt{j\omega})$, gives :

$$\left(\frac{1-C_1^2 j\omega}{1+C_1^2 j\omega}\right) = 1-2C_1^2 j\omega + O([j\omega]^2),$$

$$\frac{2C_1\sqrt{j\omega}}{\left(1+C_1^2 j\omega\right)} = 2C_1\sqrt{j\omega} - 2C_1^3\left(j\omega\right)^{3/2} + O([j\omega]^{5/2}), \tag{21}$$

and

$$\coth(LC_2\sqrt{j\omega}) = \frac{1}{LC_2\sqrt{j\omega}} + \frac{1}{3}LC_2 j\omega - \frac{1}{45}L^3C_2^3\left(j\omega\right)^{3/2} + O([j\omega]^{5/2}).$$

We have

$$\frac{2C_1\sqrt{j\omega}}{\left(1+C_1^2 j\omega\right)}\coth(LC_2\sqrt{j\omega}) = \frac{2C_1}{LC_2} + \frac{2}{3}C_1C_2L\left(1-\frac{3C_1^2}{L^2C_2^2}\right)j\omega + O([j\omega]^2),$$

and

$$\frac{1}{1+\frac{2C_1\sqrt{j\omega}}{\left(1+C_1^2 j\omega\right)}\coth(LC_2\sqrt{j\omega})} = \frac{1}{1+\frac{2C_1}{LC_2}} - \frac{2}{3}\frac{L^2C_2^2C_1\left(1-\frac{3C_1^2}{L^2C_2^2}\right)}{\left(1+\frac{2C_1}{LC_2}\right)^2}j\omega + O([j\omega]^2) \tag{22}$$

Using Eqs. (21) and (22), one finds

$$\tilde{R}(\omega) = \left(\frac{1}{1+\frac{2C_1}{LC_2}}\right)\left(1-\frac{2}{3}\frac{LC_1C_2\left(1+3\frac{C_1}{LC_2}+3\frac{C_1^2}{L^2C_2^2}\right)}{1+\frac{2C_1}{LC_2}}j\omega + O([j\omega]^2)\right).$$

which is equivalent to Eq. 7.

REFERENCES

[1]J. F. Allard, *Propagation of Sound in Porous Media Modelling. Sound Absorbing Materials* (Elsevier, London, UK, 1993), pp. 1-284.

[2]D. Lafarge, *Materials and Acoustics Handbook*, (M. Bruneau and C. Potel eds, ISTE-Wiley, London, 2009), pp. 149-202.

[3]M.E. Delany and E.N. Bazley, "Acoustical properties of fibrous materials", Appl. Acoust. **3**, 105 (1970).

[4]Y. Miki, "Acoustical properties of porous materials Modification of Delaney Bazeley models", J. Acoust. Soc. Jpn. (E) **11**, 19 (1990).

[5]D.A. Bies and C.H. Hansen, "Flow resistance information for acoustical design", Appl. Acoust. **13**, 357 (1980).

[6]D.L. Johnson, J. Koplik and R. Dashen, "Theory of dynamic permeability and tortuosity in fluid-saturated porous media", J. Fluid.Mech. **176**, 379 (1987).

[7]M. Sadouki, Z.E.A. Fellah, A. Berbiche. M. Fellah, F.G. Mitri, E. Ogam and C. Depollier, Measuring static viscous permeability of porous absorbing materials, J. Acoust. Soc. Am. **135**, 3163 (2014).

[8]R.L. Brown and R.H. Bolt, "The measurement of flow resistance of porous acoustic materials", J. Acoust. Soc. Am. **13**, 337 (1942).

[9]R.W. Leonard, "Simplified flow resistance measurements", J. Acoust. Soc. Am. **17**, 240 (1946).

[10]M.R. Stinson and G.A. Daigle, "Electronic system for the measurement of flow resistance", J. Acoust. Soc. Am. **83**, 2422 (1988).

[11]ISO 9053, Acoustics-Materials for acoustical applications-Determination of airflow resistance (ISO, 1991).

[12]ASTM C 522, Airflow Resistance of Acoustical Materials (ASTM, 2003).

[13]K. U. Ingard and T. A. Dear, "Measurement of acoustic flow resistance," J. Sound Vib. 103(4), 567 (1985).

[14]R. Woodcock and M. Hodgson, "Acoustic methods for determining the effective flow resistivity of fibrous materials," J. Sound Vib. 153(1), 186 (1992).

[15]M. Ren and F. Jacobsen, "Method of measuring the dynamic flow resistance and reactance of porous materials," Appl. Acoust. 39, 256 (1993).

[16]M. A. Picard, P. Solana, and J. F. Urchueguia, "A method of measuring the dynamic flow resistance and the acoustic measurement of the effective static flow resistance in stratified rockwool samples," J. Sound Vib. 216(3), 495 (1998).

[17]R. Panneton and X. Olny, "Acoustical determination of the parameters governing viscous dissipation in porous media," J. Acoust. Soc. Am. 119(4), 2027 (2006).

[18]O. Doutres, Y. Salissou, N. Atalla, and R. Panneton, "Evaluation of the acoustic and non-acoustic properties of sound absorbing materials using a three-microphone impedance tube," Appl. Acoust. 71(6), 506(2010).

[19]N. Sebaa, Z.E.A. Fellah, M. Fellah, W. Lauriks and C. Depollier, "Measuring flow resistivity of porous material via acoustic reflected waves", J. Appl. Phys. **98**, 084901 (2005).

[20]Z.E.A. Fellah, M. Fellah, N. Sebaa, W. Lauriks and C. Depollier, "Measuring flow resistivity of porous materials at low frequencies range via acoustic transmitted waves" J. Acoust. Soc. Am. **119**, 1926 (2006).

[21]Z.E.A. Fellah, M. Fellah, F.G. Mitri, N. Sebaa, C. Depollier, W. Lauriks, "Measuring permeability of porous materials at low frequency range via acoustic transmitted waves", Rev. Sci. Instrum. **78**, 114902 (2007).

[22]L. Lin, M. L. Peterson, A. R. Greenberg, B. A. McCool, "In situ measurement of permeability", J. Acoust. Soc. Am. **125**, (4) EL 123-EL 128 (2009).

[23]R. Dragonetti, C. Ianniello, and A.R. Romano, "Measurement of the resistivity of porous materials with an alternating air-flow method" J. Acoust. Soc. Am. **129**, 753 (2010).

[24]J. P. Arenas, R.D Rey, J. Alba and J. Ramis, "Evaluation of two alternative procedures for measuring airflow resistance of sound absorbing materials" ICSV20, Bangkok, Thailand, 7-11 July (2013).

[25]M. A. Biot, "The theory of propagation of elastic waves in fluid-saturated porous solid. I. Low frequency range," J. Acoust. Soc. Am. 28, 168 (1956).

[26]Z.E.A. Fellah and C. Depollier, "Transient wave propagation in rigid porous media : a time domain approach", J. Acoust. Soc. Am., **107**, 683 (2000).

[27] J.M. Carcione, "Wave propagation in anisotropic, saturated porous media : Plane-wave theory and numerical simulation", J. Acoust. Soc. Am., **99**, 2655 (1996).

[28]M.J.Y. Ou, "On reconstruction of dynamic permeability and tortuosity from data at distinct frequencies", Inverse Problems, **30**, 095002 (2014).

Table I. Values of (ω/ω_c) and $\mid \tilde{R}(\omega) \mid$ for different values of frequency and resistivity, the thickness is fixed to $L = 5cm$.

	30 Hz		50 Hz		70 Hz		100 Hz		200 Hz		300 Hz	
$\sigma\ (Nm^{-4}s)$	ω/ω_c	$\mid \tilde{R} \mid$	ω/ω_c	$\mid \tilde{R} \mid$	ω/ω_c	$\mid \tilde{R} \mid$	ω/ω_c	$\mid \tilde{R} \mid$	ω/ω_c	$\mid \tilde{R} \mid$	ω/ω_c	$\mid \tilde{R} \mid$
3000	0.113	0.155	0.189	0.157	0.264	0.159	0.377	0.165	0.755	0.193	1.132	0.233
10^4	0.048	0.379	0.080	0.380	0.112	0.381	0.160	0.383	0.320	0.398	0.480	0.420
10^5	0.025	0.859	0.042	0.860	0.059	0.860	0.084	0.862	0.168	0.871	0.252	0.886
10^6	0.023	0.984	0.039	0.984	0.054	0.985	0.078	0.987	0.156	0.996	0.233	1.01
	400 Hz		500 Hz		600 Hz		700 Hz		800 Hz		1000 Hz	
$\sigma\ (Nm^{-4}s)$	ω/ω_c	$\mid \tilde{R} \mid$	ω/ω_c	$\mid \tilde{R} \mid$	ω/ω_c	$\mid \tilde{R} \mid$	ω/ω_c	$\mid \tilde{R} \mid$	ω/ω_c	$\mid \tilde{R} \mid$	ω/ω_c	$\mid \tilde{R} \mid$
3000	1.509	0.280	1.887	0.330	2.264	0.382	2.642	0.436	3.016	0.492	3.774	0.604
10^4	0.641	0.450	0.801	0.485	0.961	0.525	1.121	0.569	1.281	0.615	1.601	0.715
10^5	0.336	0.906	0.420	0.932	0.504	0.962	0.588	0.996	0.672	1.035	0.840	1.122
10^6	0.311	1.030	0.389	1.056	0.467	1.086	0.545	1.120	0.623	1.159	0.778	1.247

Table II. Porosities and thicknesses of the samples M1-M4.

Material	M1	M2	M3	M4
Thickness (cm)	2.6	5	4.15	4.9
Porosity	0.85	0.95	0.8	0.98

Table III. Characteristics of sample M1 obtained by solving the inverse problem using the general and simplified expression (Eq. 4 and 9) of the reflection coefficient (not marked), either by classical methods (marked by $*$), or by taking an average of the inverted values (marked by $\sharp$).

Frequency bandwidths(Hz)	(40-60)	(50-70)	(60-80)	(70-90)	(80-100)	(90-120)		
k_0 (Eq. 4) *Darcy*	672.68	568.30	757.73	835.05	734.53	734.53	$717.66^{\sharp}$	720^{*}
k_0 (Eq. 9) *Darcy*	672.68	568.30	757.73	835.05	730.00	729.53	$715.54^{\sharp}$	720^{*}
σ (Eq. 4) $\mathrm{Nm}^{-4}\mathrm{s}$	27508	32650	24490	22220	25260	25260	$25857^{\sharp}$	25773^{*}
σ (Eq. 9) $\mathrm{Nm}^{-4}\mathrm{s}$	27508	32650	24490	22220	25420	25436	$25934^{\sharp}$	25773^{*}

Table IV. Characteristics of sample M2 obtained by solving the inverse problem using the general and simplified expression (Eq. 4 and 9) of the reflection coefficient (not marked), either by classical methods (marked by $*$), or by taking an average of the inverted values (marked by $\sharp$).

Frequency bandwidths(Hz)	(40-60)	(50-70)	(60-80)	(70-90)	(80-100)	(90-120)		
k_0 (Eq. 4)$Darcy$	2536.1	2024.2	2171.0	3131.4	2610.7	2690.7	$2527^{\sharp}$	2900^{*}
k_0 (Eq. 9)$Darcy$	2536.1	2103.1	2250.0	3131.4	2690.7	2690.7	$2567^{\sharp}$	2900^{*}
σ (Eq. 4) $\mathrm{Nm^{-4}s}$	7320	9163	8539	5930	7101	6890	$7348.3^{\sharp}$	6398^{*}
σ (Eq. 9) $\mathrm{Nm^{-4}s}$	7320	8820	8240	5930	6890	6890	$7339.7^{\sharp}$	6398^{*}

Table V. Characteristics of sample M3 obtained by solving the inverse problem using the general and simplified expression (Eq. 4 and 9) of the reflection coefficient (not marked), either by classical methods (marked by $*$), or by taking an average of the inverted values (marked by $\sharp$).

Frequency bandwidths(Hz)	(40-60)	(50-70)	(60-80)	(70-90)	(80-100)	(90-120)		
k_0 (Eq. 4)$Darcy$	618.55	541.23	657.21	594.1	594.3	568.67	$595.6^{\sharp}$	630^{*}
k_0 (Eq. 9)$Darcy$	618.55	541.23	657.21	599.22	599.22	579.89	$599.2^{\sharp}$	630^{*}
σ (Eq. 4) $\mathrm{Nm^{-4}s}$	30000	34280	28230	30960	30960	32000	$31072^{\sharp}$	29455^{*}
σ (Eq. 4) $\mathrm{Nm^{-4}s}$	30000	34280	28230	30960	30960	32000	$31216^{\sharp}$	29455^{*}

Table VI. Characteristics of sample M4 obtained by solving the inverse problem using the general and simplified expression (Eq. 4 and 9) of the reflection coefficient (not marked), either by classical methods (marked by $*$), or by taking an average of the inverted values (marked by $\sharp$).

Frequency bandwidths(Hz)	(40-60)	(50-70)	(60-80)	(70-90)	(80-100)	(90-120)		
k_0 (Eq. 4)$Darcy$	5613.4	3943.3	4360.8	3943.3	4195.1	4702.6	$4460^{\sharp}$	4500^{*}
k_0 (Eq. 9)$Darcy$	5613.4	3943.3	4360.8	3943.3	4360.8	4778.4	$4500^{\sharp}$	4500^{*}
σ (Eq. 4) $\mathrm{Nm^{-4}s}$	3310	4700	4250	4700	4417	3943	$4219.2^{\sharp}$	4123.7^{*}
σ (Eq. 9) $\mathrm{Nm^{-4}s}$	3310	4700	4250	4700	4250	3880	$4181.7^{\sharp}$	4123.7^{*}

Table VII. Standard deviation of permeability.

Materials	Permeability k_0 $(Darcy)$	Standard deviation
M1	717,66$^\sharp$	77.22
M2	2567$^\sharp$	512.58
M3	599.2$^\sharp$	35.62
M4	4500$^\sharp$	573.83

FIGURE CAPTIONS

Fig. 1. Variation of the modulus of the reflection coefficient with porosity.

Fig. 2. (Color online) Comparison between simulated reflected signals corresponding to Eq.(5) (solid line) and Eq.(9) (dashed line), for the sample F1.

Fig. 3. (Color online) Comparison between simulated reflected signals corresponding to Eq. (5) (solid line) and Eq. (9) (dashed line), for the sample F2.

Fig. 4. (Color online) Comparison between simulated reflected signals corresponding to Eq. (5) (solid line) and Eq. (9) (dashed line), for the sample F1, in the frequency band (40-70)Hz.

Fig. 5. (Color online) Comparison between simulated reflected signals corresponding to Eq. (5) (solid line) and Eq. (9) (dashed line), for the sample F2, in the frequency band (40-70)Hz.

Fig. 6. Experimental setup of acoustic measurements.

Fig. 7. (Color online) Variations of the cost (minimization) function with the static permeability k_0 for different frequency bandwidths (sample M1).

Fig. 8. (Color online) Variations of the cost (minimization) function with the static permeability k_0 for different frequency bandwidths (sample M2).

Fig. 9. (Color online) Variations of the cost (minimization) function with the static permeability k_0 for different frequency bandwidths (sample M3).

Fig. 10. (Color online) Variations of the cost (minimization) function with the static permeability k_0 for different frequency bandwidths (sample M4).

Fig. 11-a. (Color online) Comparison between the experimental reflected signal (dashed line) and the simulated reflected signals (solid line) using the reconstructed value of k_0, for the sample M1 in the frequency bandwidth (40-60)Hz.

Fig. 11-b. (Color online) Comparison between the experimental reflected signal (dashed line) and the simulated reflected signals (solid line) using the reconstructed value of k_0, for the sample M2 in the frequency bandwidth (40-60)Hz.

Fig. 11-c. (Color online) Comparison between the experimental reflected signal (dashed line) and the simulated reflected signals (solid line) using the reconstructed value of k_0, for the sample M3 in the frequency bandwidth (40-60)Hz.

Fig. 11-d. (Color online) Comparison between the experimental reflected signal (dashed line) and the simulated reflected signals (solid line) using the reconstructed value of k_0, for the sample M4 in the frequency bandwidth (40-60)Hz.

Fig. 12-a. (Color online) Comparison between the experimental reflected signal (dashed line) and the simulated reflected signals (solid line) using the reconstructed value of k_0, for the sample M1 in the frequency bandwidth (90-120)Hz.

Fig. 12-b. (Color online) Comparison between the experimental reflected signal (dashed line) and the simulated reflected signals (solid line) using the reconstructed value of k_0, for the sample

M2 in the frequency bandwidth (90-120)Hz.

Fig. 12-c. (Color online) Comparison between the experimental reflected signal (dashed line) and the simulated reflected signals (solid line) using the reconstructed value of k_0, for the sample M3 in the frequency bandwidth (90-120)Hz.

Fig. 12-d. (Color online) Comparison between the experimental reflected signal (dashed line) and the simulated reflected signals (solid line) using the reconstructed value of k_0, for the sample M4 in the frequency bandwidth (90-120)Hz.

Fig. 13. Problem geometry.

Fig. 1

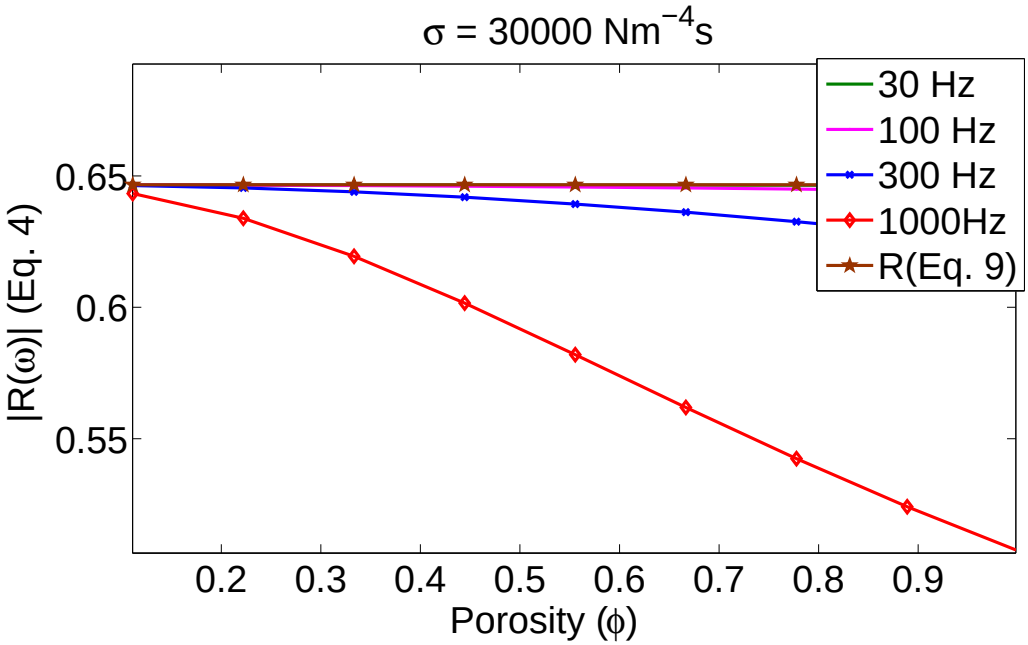
σ = 30000 Nm^{-4}s
30 Hz
100 Hz
300 Hz
1000Hz
R(Eq. 9)
|R(ω)| (Eq. 4)
0.65
0.6
0.55
0.2
0.3
0.4
0.5
0.6
0.7
0.8
0.9
Porosity (ϕ)

Fig. 2

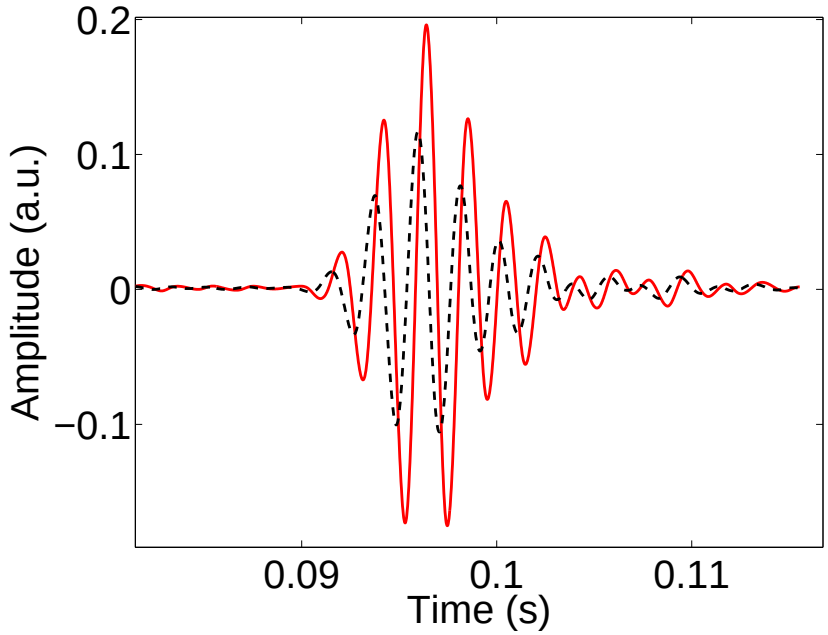

Fig. 3

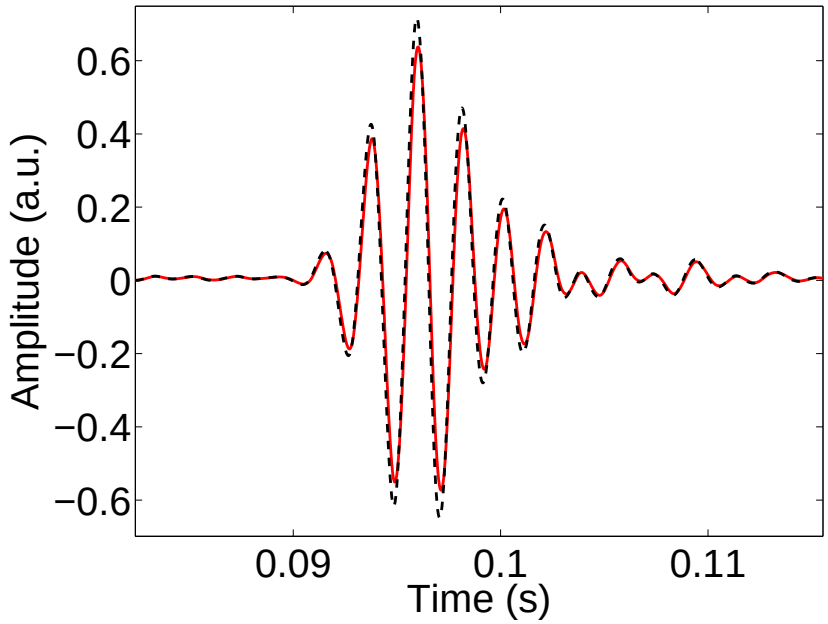

Fig. 4

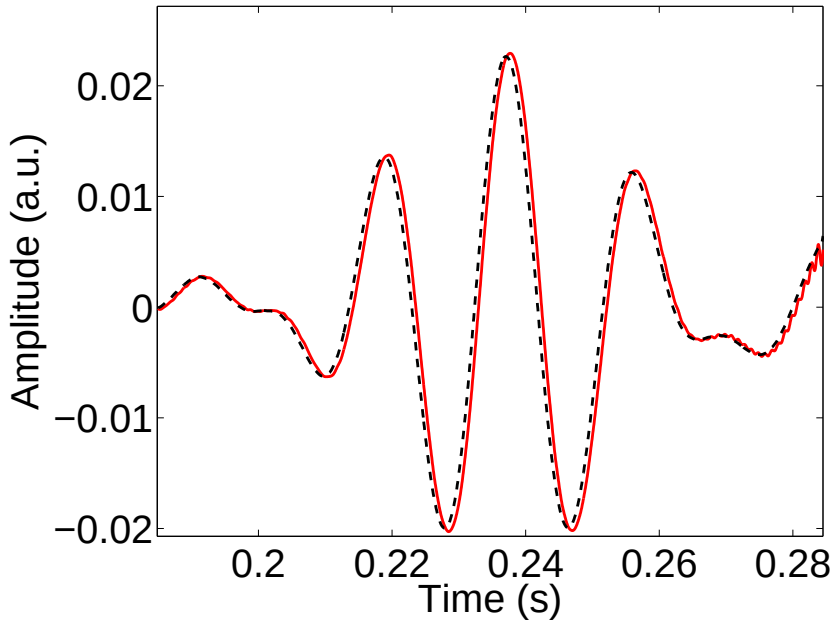

Fig. 5

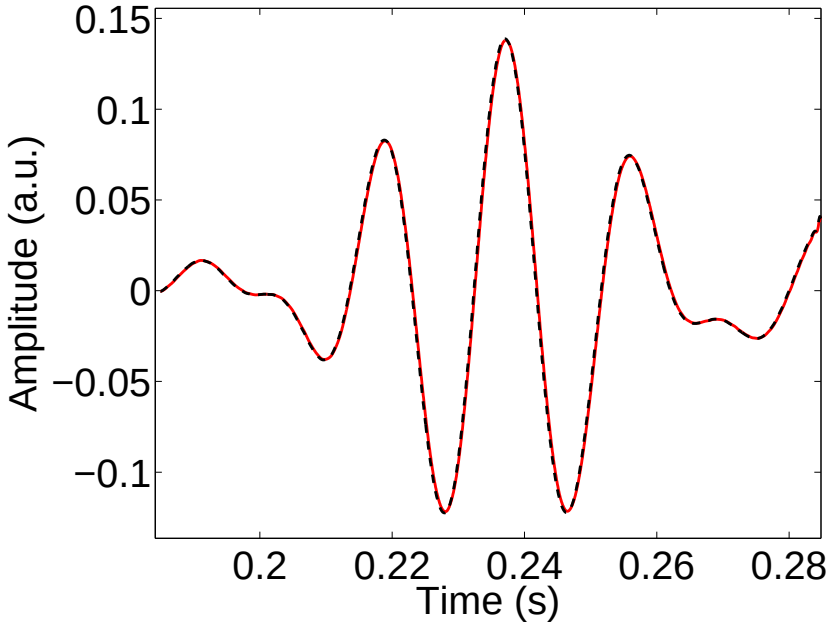

Fig. 6

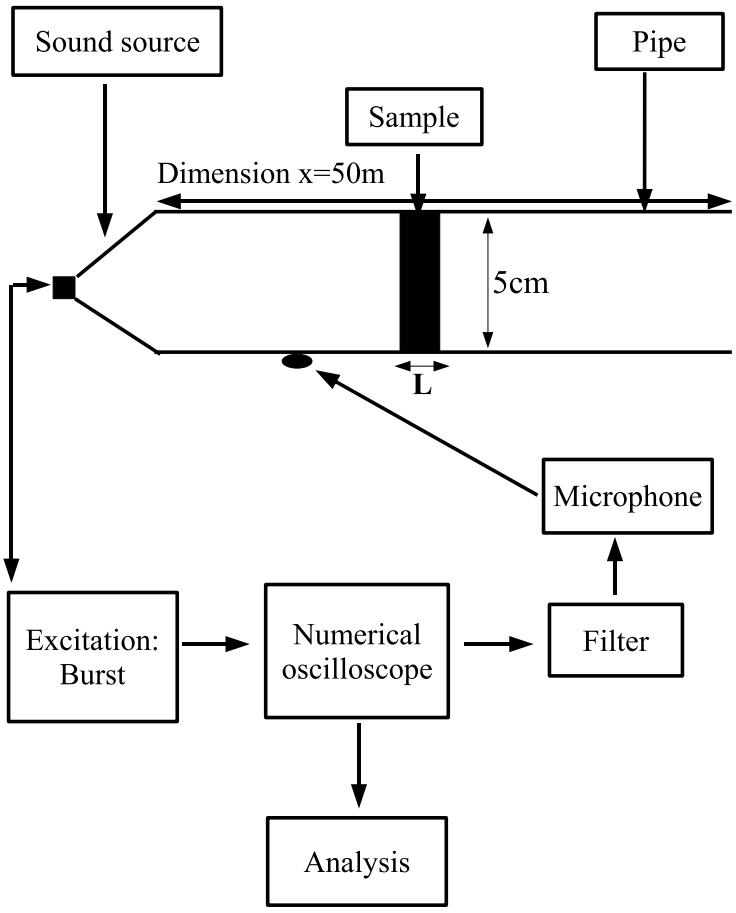
Sound source
Pipe
Sample
Dimension x=50m
5cm
L
Microphone
Excitation:
Burst
Numerical
oscilloscope
Filter
Analysis

Fig. 7

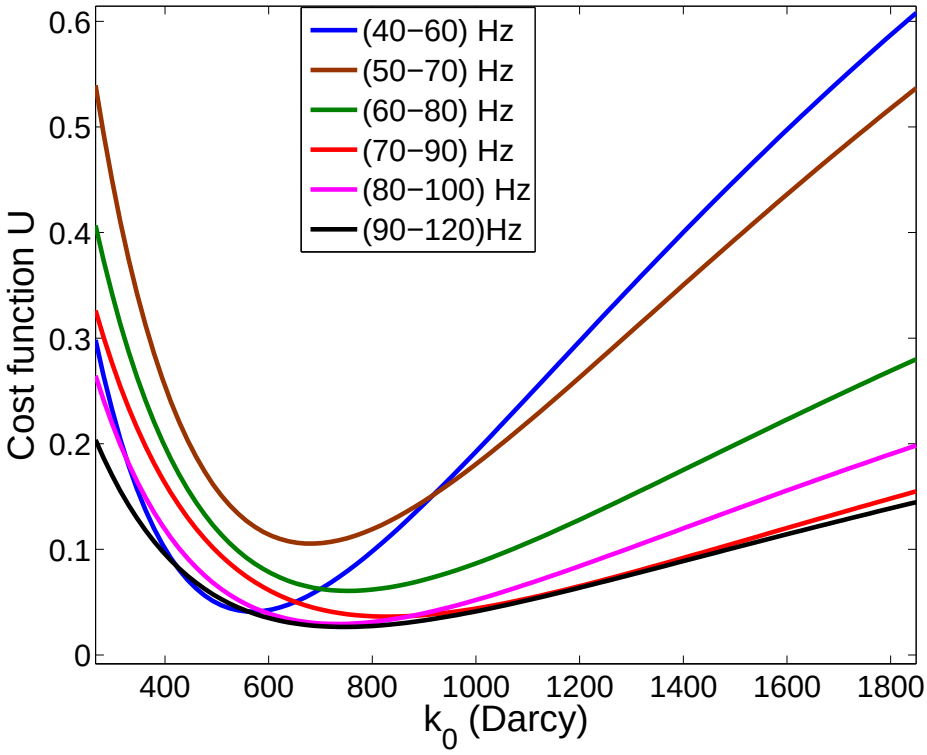
(40−60) Hz
(50−70) Hz
(60−80) Hz
(70−90) Hz
(80−100) Hz
(90−120)Hz
Cost function U
0
0.1
0.2
0.3
0.4
0.5
0.6
400
600
800
1000
1200
1400
1600
1800
k0 (Darcy)

Fig. 8

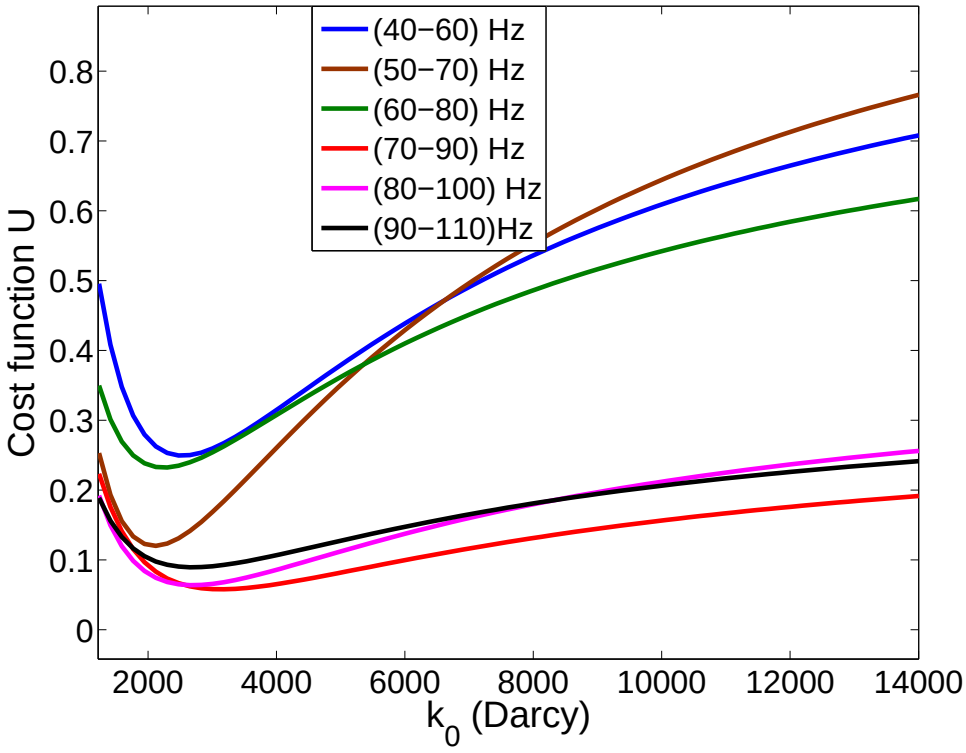
(40−60) Hz
(50−70) Hz
(60−80) Hz
(70−90) Hz
(80−100) Hz
(90−110)Hz
Cost function U
0
0.1
0.2
0.3
0.4
0.5
0.6
0.7
0.8
2000
4000
6000
8000
10000
12000
14000
k0 (Darcy)

Fig.9

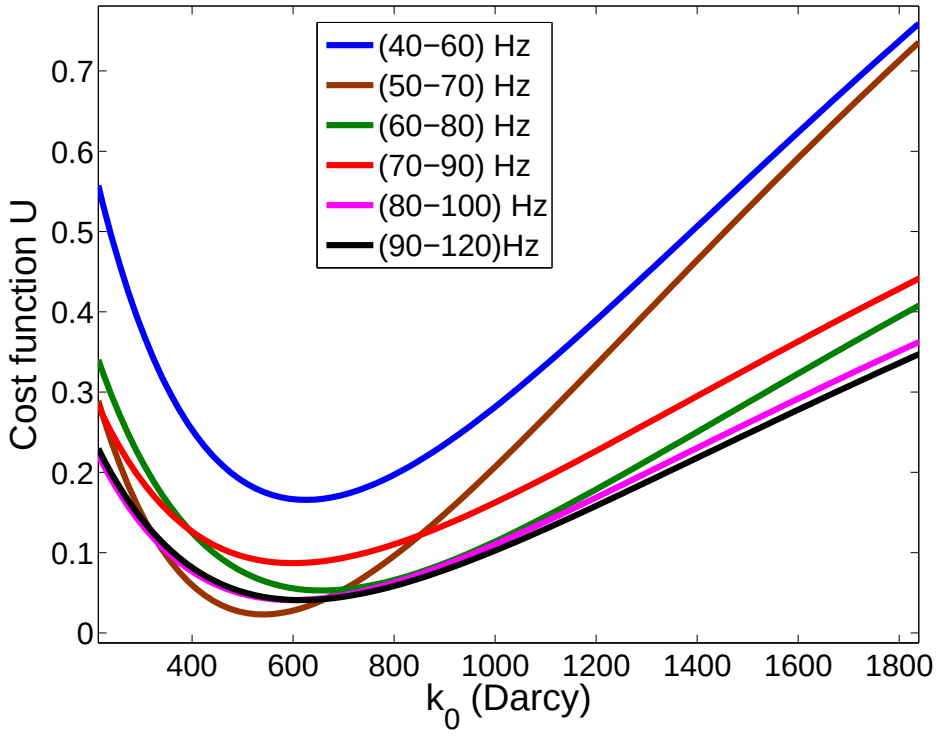
(40−60) Hz
(50−70) Hz
(60−80) Hz
(70−90) Hz
(80−100) Hz
(90−120)Hz
Cost function U
0
0.1
0.2
0.3
0.4
0.5
0.6
0.7
400
600
800
1000
1200
1400
1600
1800
k0 (Darcy)

Fig. 10

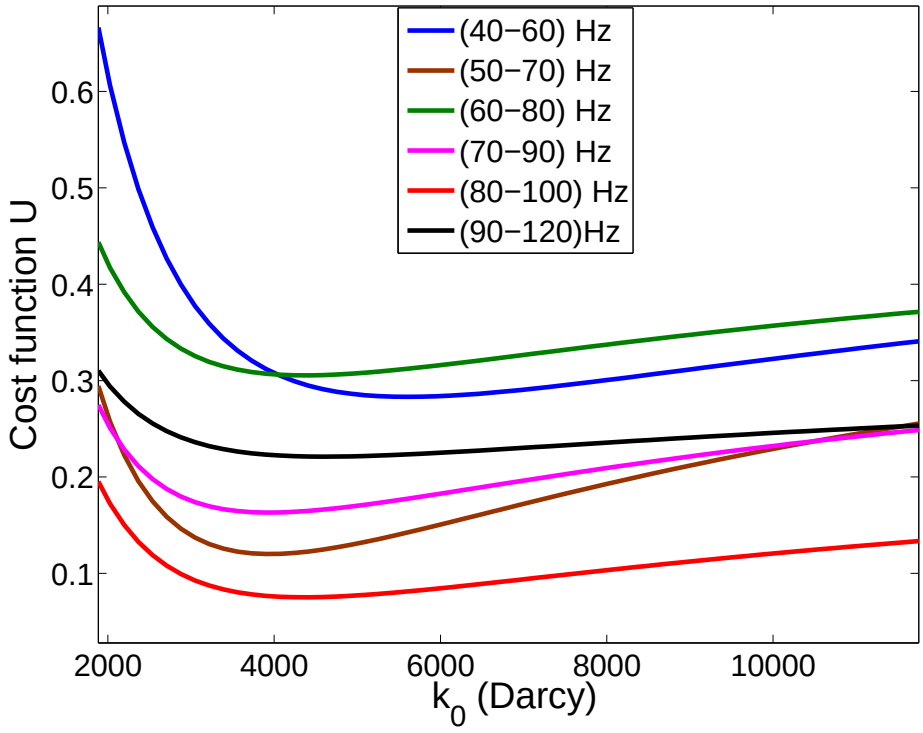
(40−60) Hz
(50−70) Hz
(60−80) Hz
(70−90) Hz
(80−100) Hz
(90−120)Hz
Cost function U
0.6
0.5
0.4
0.3
0.2
0.1
2000
4000
6000
8000
10000
k0 (Darcy)

Fig. 11-a

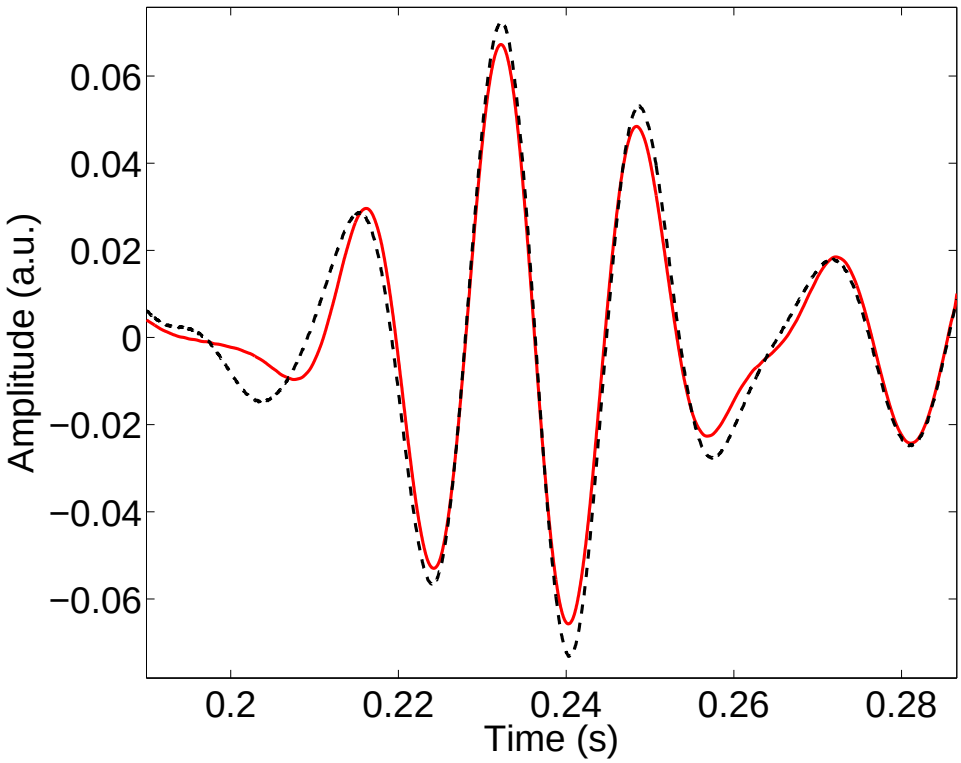

Fig. 11-b

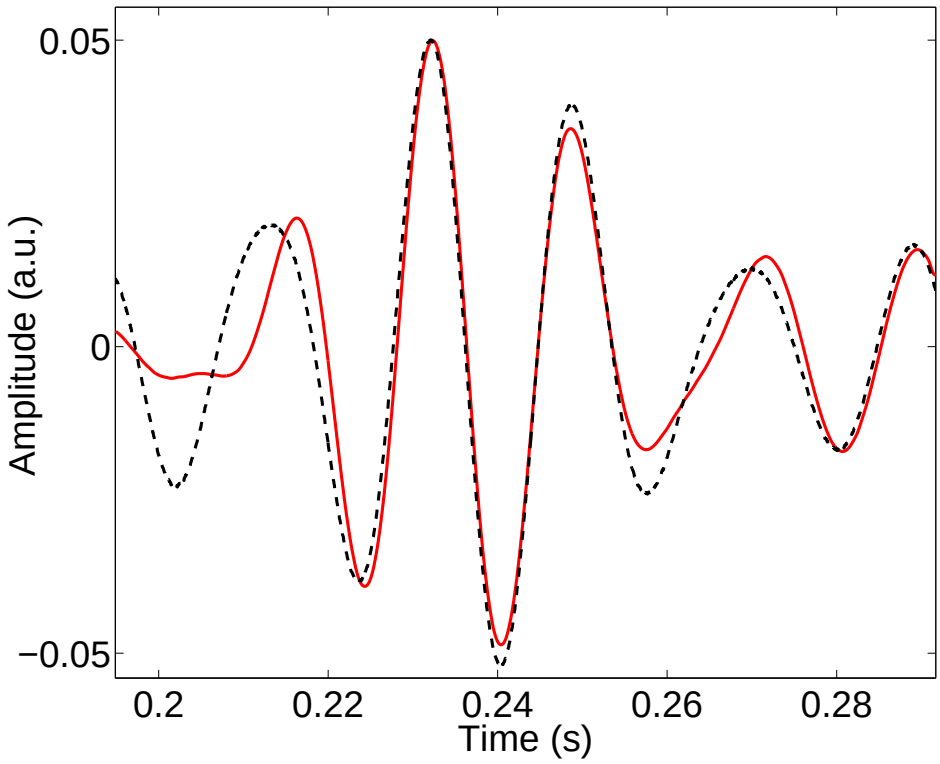

Fig. 11-c

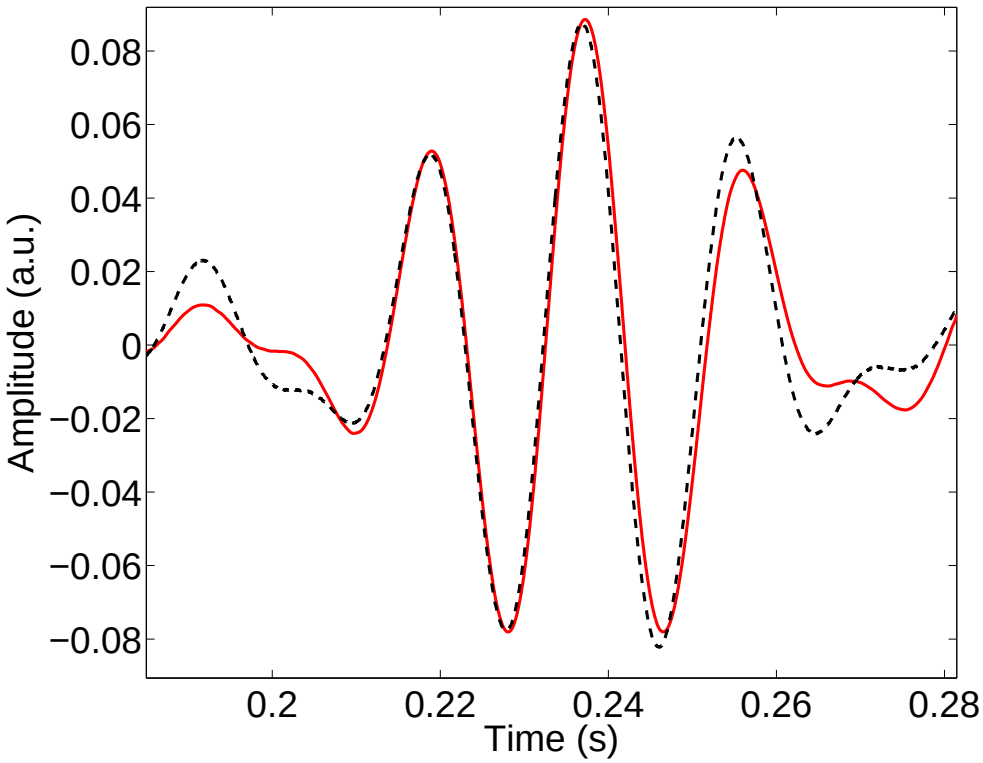
0.08
0.06
0.04
0.02
0
−0.02
−0.04
−0.06
−0.08
Amplitude (a.u.)
0.2
0.22
0.24
0.26
0.28
Time (s)

Fig. 11-d

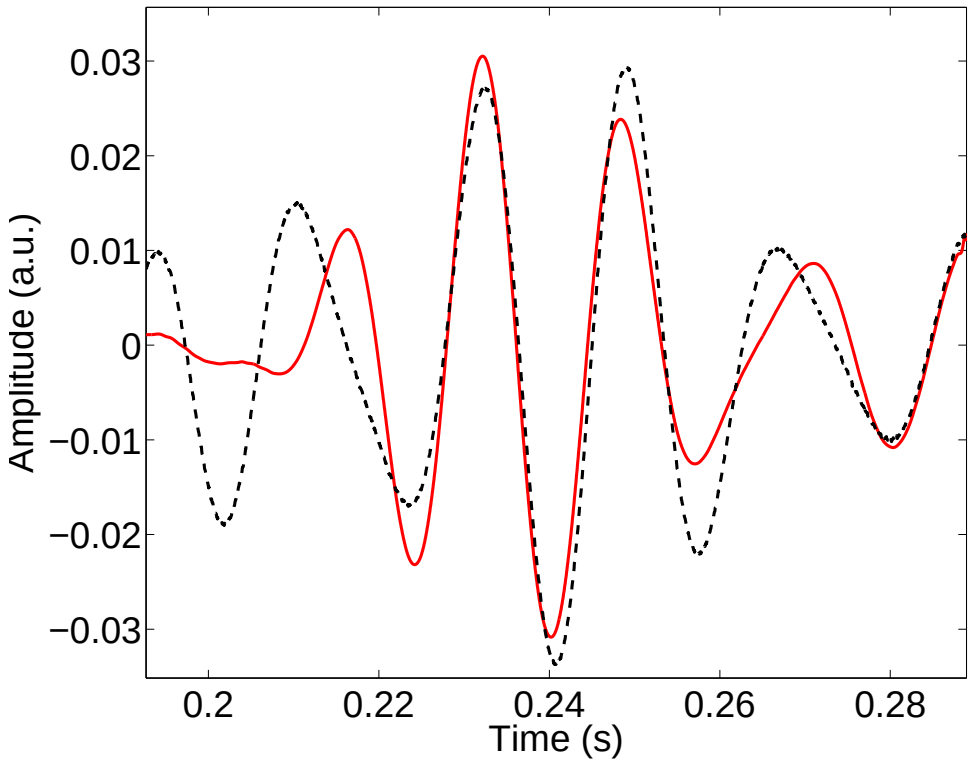

Fig. 12-a

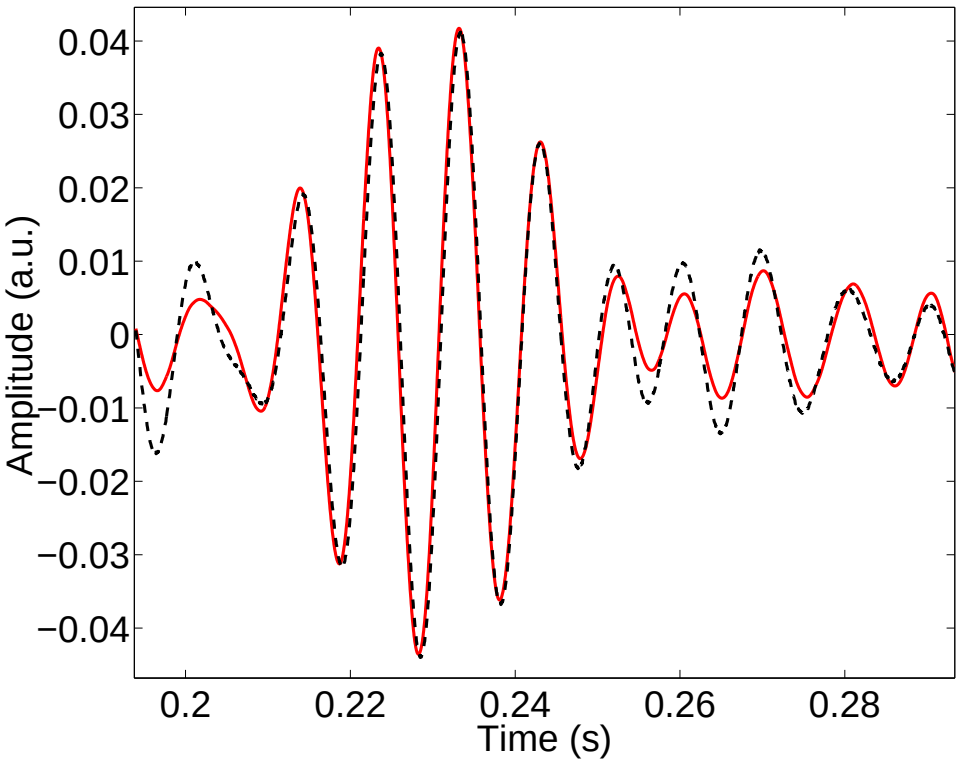
0.04
0.03
0.02
0.01
0
−0.01
−0.02
−0.03
−0.04
Amplitude (a.u.)
0.2
0.22
0.24
0.26
0.28
Time (s)

Fig. 12-b

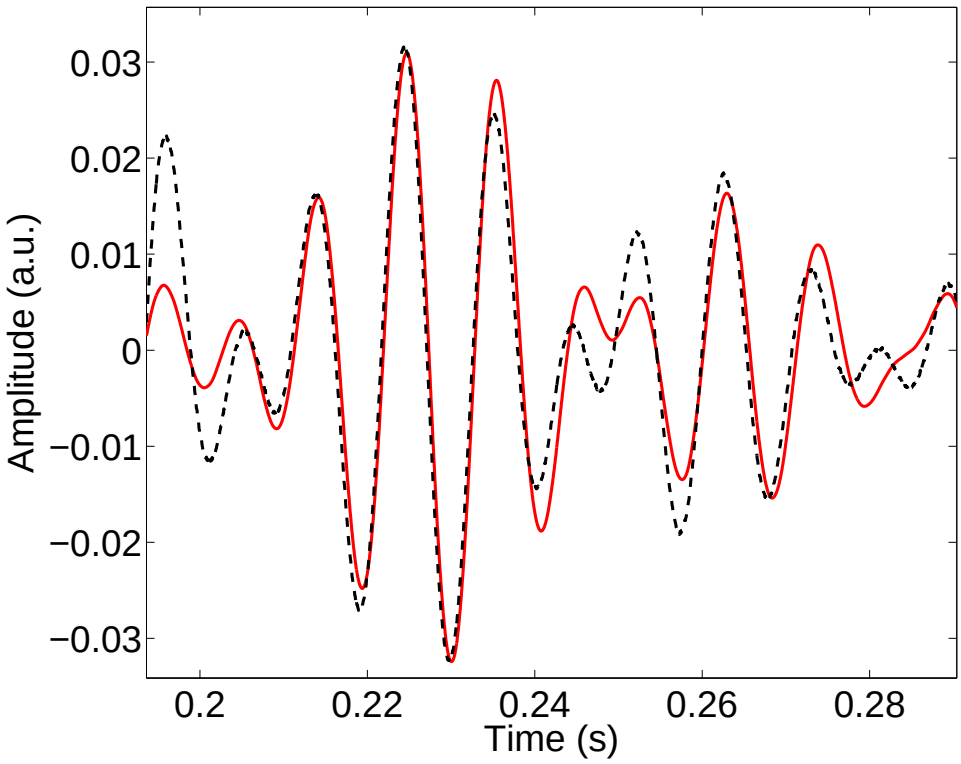

Fig. 12-c

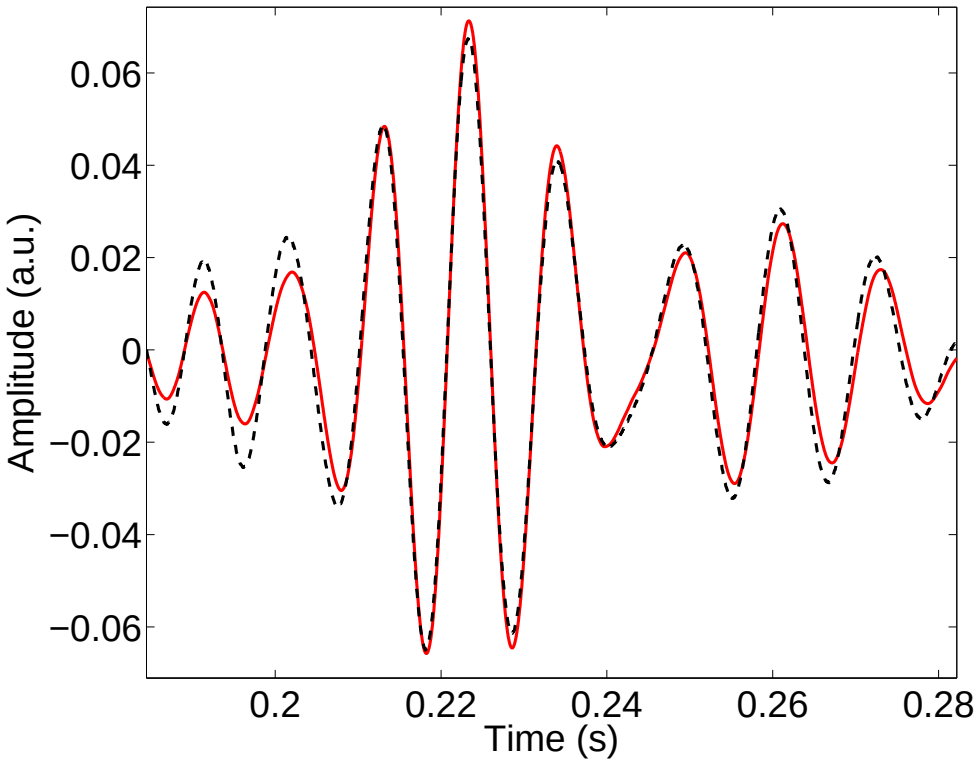

Fig. 12-d

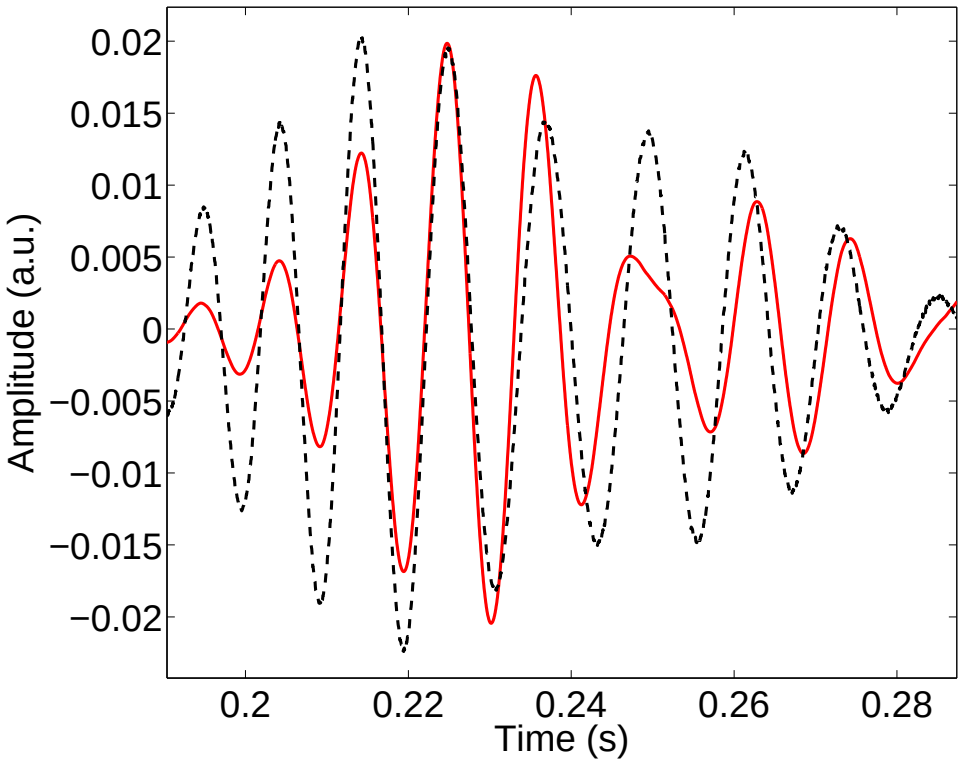
0.02
0.015
0.01
0.005
0
−0.005
−0.01
−0.015
−0.02
Amplitude (a.u.)
0.2
0.22
0.24
0.26
0.28
Time (s)

Fig. 13

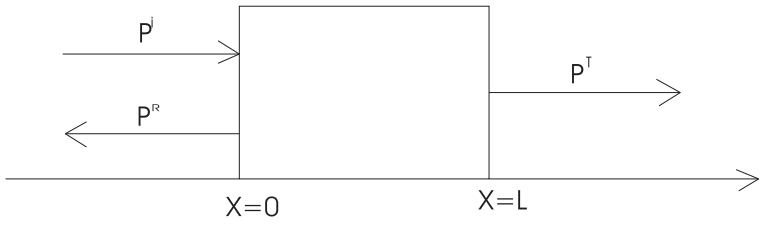

FIGURE 1 –